



Design of a novel wideband microstrip diplexer using artificial neural network

Abbas Rezaei¹ · Salah I. Yahya^{2,3} · Leila Noori⁴ · Mohd Haizal Jamaluddin⁵

Received: 9 May 2019 / Revised: 9 May 2019 / Accepted: 16 July 2019 / Published online: 22 July 2019
© Springer Science+Business Media, LLC, part of Springer Nature 2019

Abstract

In this paper, we use an artificial neural network (ANN) to design a compact microstrip diplexer with wide fractional bandwidths (FBW) for wideband applications. For this purpose, a multilayer perceptron neural network model trained with the back-propagation algorithm is used. First, a novel resonator consists of coupled lines loaded by similar patch cells is proposed. Then, using the proposed ANN model, two mathematical equations for S_{11} and S_{21} are obtained to achieve the best configuration of the proposed bandpass filters and tune their resonant frequencies. Finally, using the obtained bandpass filters, a high-performance microstrip diplexer is created. The first channel of the diplexer is from 1.47 GHz up to 1.74 GHz with a wide FBW of 16.8%. The second channel is expanded from 2 to 2.23 GHz with a fractional bandwidth of 11%. In comparison with the previous designs, our diplexer has the most compact size. Moreover, the insertion losses at both channels are improved so that they are 0.1 dB and 0.16 dB at the lower and upper channels, respectively. Both channels are flat with a maximum group delay of 2.6 ns, which makes it suitable for high data rate communication links. To validate the designing method and simulation results, the presented diplexer is fabricated and measured.

Keywords Microstrip · Diplexer · Compact · Ultra-wideband · Artificial neural network · Multilayer Perceptron

1 Introduction

A microstrip diplexer implements frequency-domain multiplexing. Therefore, a planar high-performance diplexer with a compact size is widely demanded by the modern wireless communication systems. A high data-rate communication link is forced to employ wide passbands. To obtain an important advantage, a link with low data rate may deliberately use a wider bandwidth too. Ultra-wideband (UWB) is a technology to transmit data over a large bandwidth (> 0.5 GHz). Accordingly, a diplexer with wide bandwidths (having the high data-rate capability) can play a key role in UWB communication systems.

Several types of microstrip diplexers have been introduced for various applications [1–19]. However, they have relatively narrow bandwidths and occupied large areas. The proposed diplexers in [1, 2] have low insertion losses at both channels while in [1] the frequency selectivity at the upper channel is relatively poor. Using common shorted stubs, a microstrip diplexer has been presented in [3]. It has several transmission zeros at the stopband. It operates at

✉ Abbas Rezaei
a.rezaee@kut.ac.ir

Salah I. Yahya
salah.ismaeel@koyauniversity.org

Leila Noori
leila_noori62@yahoo.com

Mohd Haizal Jamaluddin
haizal@fke.utm.my

¹ Department of Electrical Engineering, Kermanshah University of Technology, Kermanshah, Iran
² Department of Software Engineering, Faculty of Engineering, Koya University, Koya, Kurdistan Region KOY45, Iraq
³ Department of Computer Science and Engineering, University of Kurdistan Hewler, Erbil, Kurdistan Region, Iraq
⁴ Department of Electrical and Electronics Engineering, Shiraz University of Technology, Shiraz, Iran
⁵ Wireless Communication Centre, School of Electrical Engineering, Universiti Teknologi Malaysia, Johor, Malaysia

2.4 GHz and 1.8 GHz for WLAN and GSM applications, respectively.

Nevertheless, the introduced diplexers in [3–16] could not decrease the insertion losses acceptably. In [4] and [5], coupled stepped impedance resonators and interdigital capacitors have been utilized, respectively, to design microstrip diplexers working at GSM and WLAN frequency bands. A diplexer has been designed in [6] based on a novel microstrip structure using four coupled lines integrated by step impedance cells, but it has low isolation. An unbalanced-to-balanced microstrip diplexer has been presented in [7] based on stub-loaded dual-mode resonators.

In [8], the coupled lines have been integrated to create a diplexer with several transmission zeros, which improve the stopband properties. In [9], microstrip triangular open-loop resonators have been employed to achieve a diplexer for the 4G application. A microstrip ring resonator coupled to the transmission lines has been used in [10]. In comparison to the other reported diplexers, it could expand the bandwidth slightly.

In [11], a high isolation diplexer has been designed using coupled square and rectangular open-loop resonators. To obtain a dual-frequency diplexer operated at 1.95 GHz and 2.14 GHz, two stub-loaded U-shape resonators have been integrated by a T-shape junction in [12]. In [13], two channels have been constructed by the electrically-coupling half-wavelength resonators, which have a problem of low selectivity at upper passband. The authors in [14] could improve the isolation between two channels using an integrated waveguide substrate.

In [15], spiral cells are coupled to design a diplexer with good return losses but high insertion losses at both channels. In [16], the lumped elements are loaded inside four open loops which lead to the complexity of manufacturing, a non-planar structure, increase the size and increase the measurement errors. In [20], a microstrip diplexer with two opposite very large and very narrowband widths has been proposed. It occupies a large implementation area with a high return loss in its wider channel.

Recently, artificial neural network (ANN) has been widely used in many engineering applications [21, 22]. As a powerful mathematical tool, ANN can be used in classification, patterns modeling, prediction, and optimization problems. In [23], ANN and ANFIS (adaptive neuro-fuzzy inference system) models have been developed in a microstrip subsystem to model and predict matching condition. This subsystem consists of a microstrip bandpass filter and a low noise amplifier (LNA), which can be used for WLAN applications. In [24], radial basis function (RBF) neural network has been used to design bandpass filters in shielded printed technology. For this purpose, a nonlinear equation has been obtained to relate the dimensions of the resonators to the coupling coefficients and

quality factor. In [25], an ANN method has been used for designing a microstrip bandpass filter. For this means, dimensions and S-parameters of the microstrip bandpass filter have been used as the inputs and outputs of the ANN model, respectively.

In this paper, we use an ANN technique to design a microstrip diplexer with two wide bandwidths for L-Band and S-Band applications. Using a type of ANN, i.e., multilayer perceptron (MLP) a high-performance diplexer is designed and fabricated, which can solve the problems of the other reported diplexers in terms of reducing the size and improving the insertion losses, while the other parameters are acceptable. The wide fractional bandwidths (FBWs) of the proposed diplexer make it appropriate for UWB applications. The widest FBWs are obtained in this work. Meanwhile, it has two flat passbands with low group delays that is widely demanded by the high data-rate communication links.

The design process is prepared as follows: first, a microstrip resonator is proposed based on coupled lines and patch cells. Then, an LC model of the proposed resonator is presented and analyzed to find its most effective parameters. Next, using the proposed ANN model an optimization method is performed to design two bandpass filters by tuning the resonant frequency, bandwidth and miniaturization. Finally, using the obtained bandpass filters a high-performance diplexer is designed and fabricated.

2 Proposed resonator

To create a passband channel, we need a passive LC circuit. The LC equivalent circuit of coupled lines includes several capacitors and inductors. The coupling effect can be presented by small coupling capacitors while the microstrip lines have inductance features [26]. Due to having an LC model of coupled lines, they have been used to create a bandpass frequency response. Hence, we will use the stub loaded coupled lines to obtain a bandpass frequency response. A patch cell with capacitance properties can save size. Therefore, it is suitable to join the coupled line and complete the equivalent LC circuit of a bandpass filter (BPF).

Accordingly, we prefer to select a coupled-line loaded by rectangular patch cell as shown in Fig. 1(a). For the proposed resonator, an approximated equivalent LC circuit is depicted in Fig. 1(b), where the patch cells are replaced by the capacitor C_p and the equivalent model of coupled-line includes the capacitors C_c and inductors L_c [26]. The stubs with the physical lengths l_1 and l_6 are replaced by an inductor of L_a . Similarly, we replaced the inductors L_b instead of the stubs with the physical lengths l_3 and l_4 . The LC circuit of bends and steps are ignored because they are

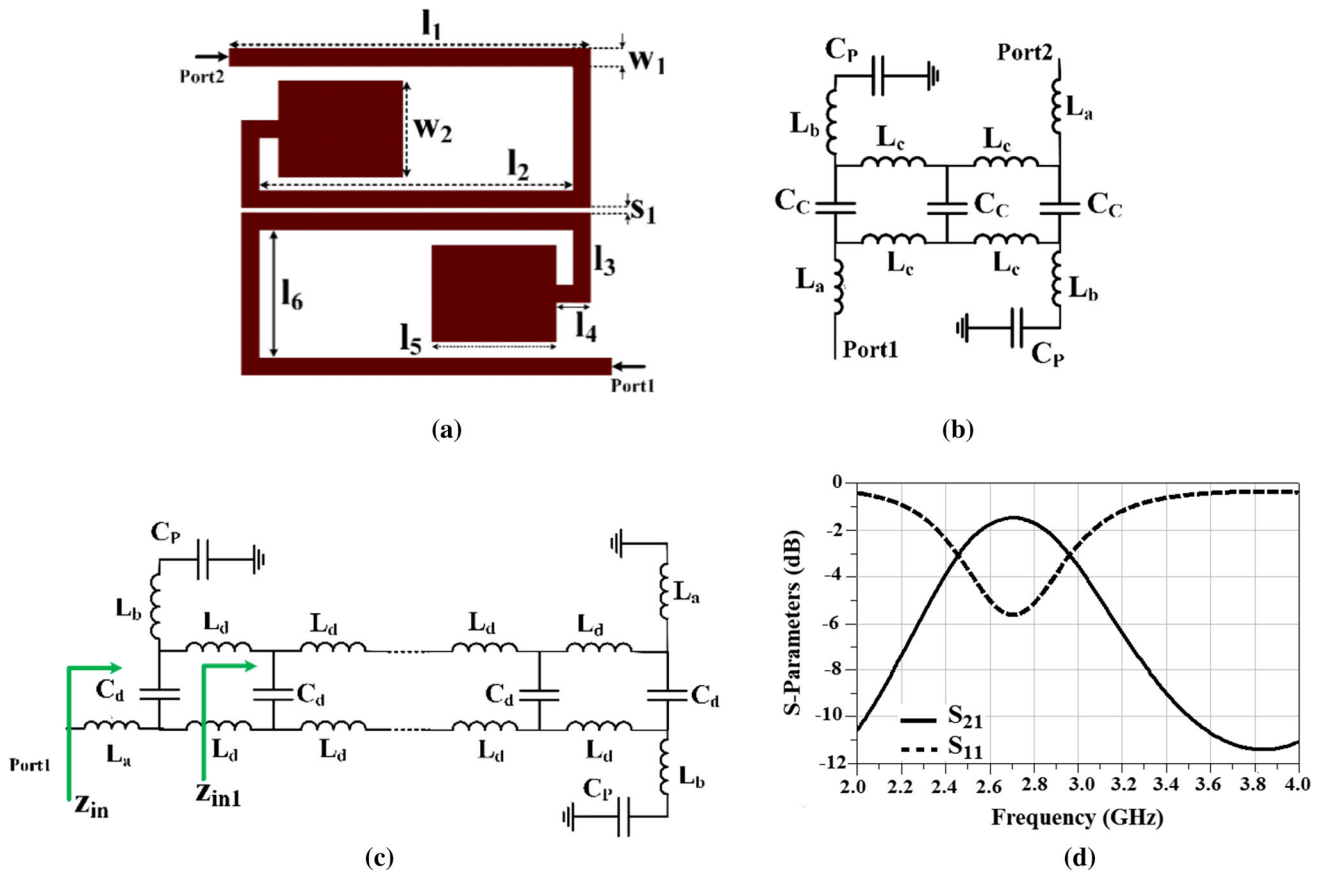


Fig. 1 Proposed resonator: **a** layout configuration, **b** LC circuit, **c** replacing the exact model of coupled lines in the LC circuit, **d** frequency response

only important at the frequencies above 10 GHz. Moreover, the equivalent circuit of the coupled lines is not exact. In the exact LC model, the number of coupling capacitors will be increased significantly.

The resonance frequency can be obtained by calculating the input impedance Z_{in} and then putting $Z_{in} = 0$. Accord-

ing to Fig. 1(c). In the exact model, an inductor of L_d is an equivalent of a small differential section of the coupled-line and the capacitors C_d depict the coupling of lines. Since the number of inductors and capacitors goes to infinity, it can be assumed that $Z_{in} \sim Z_{in1}$. According to this, the input impedance can be calculated as follows:

$$z_{in} = \frac{(z_{in} + 2\omega j L_d C_p) \times \frac{1}{j\omega C_d}}{z_{in} + 2\omega j L_d C_p + \frac{1}{j\omega C_d}} + j\omega(L_a + L_b) + \frac{1}{j\omega C_p} \Rightarrow$$

$$z_{in}^2 + z_{in} b j + c = 0 \text{ for : } \begin{cases} b = 2\omega L_d C_p + \frac{1}{\omega C_d} - \omega(L_a + L_b) \\ c = \omega^2(L_a + L_b) 2L_d C_p - 2L_d + \frac{1}{\omega^2 C_d C_p} - \frac{2L_d C_p + L_a + L_b}{C_d} \end{cases} \quad (1)$$

ingly, we have a single mode resonator achieved by having a short circuit. To calculate the input impedance Z_{in} , the approximate model is replaced by an exact model shown in

To calculate the angular resonance frequencies ω_0 , we can set $z_{in}=0$ as follows:

$$z_{in} = 0 \Rightarrow -bj \pm \sqrt{-b^2 - 4c} = 0 \Rightarrow -b \pm \sqrt{b^2 + 4c} = 0 \Rightarrow c = 0 \Rightarrow$$

$$\omega_o^4 - \frac{2L_d C_p + L_a + L_b}{2L_d C_p C_d (L_a + L_b)} \omega_o^2 + \frac{1 - 2L_d C_d C_p}{2L_d C_p^2 C_d (L_a + L_b)} = 0 \Rightarrow \quad (2)$$

$$\omega_o = \sqrt{\frac{2L_d C_p + L_a + L_b}{4L_d C_p C_d (L_a + L_b)} \left(1 \pm \sqrt{1 - 2L_d C_p^2 C_d (L_a + L_b)} \frac{1 - L_d C_p C_d (L_a + L_b)}{(2L_d C_p + L_a + L_b)^2}\right)}$$

Applying some approximations will help us to find the effective parameters in tuning resonant frequency. According to the transmission line formulas, when the inductors L_a and L_b are with millimetric dimensions, they are usually in nH, but L_d is the smaller parameter. On the other hand, the coupling capacitors are very small in PF. These estimates are based on the approximated dimensions of the microstrip lines that we usually set them in mm. Based on the above discussion, applying two approximations leads to the following simplifications:

dimensions of them will be selected to obtain a target resonant frequency by Eq. (4).

Knowing the behavior of the resonator will help in the diplexer design. Using this method, the resonant frequency will be tuned without size increment. The frequency response of the proposed resonator is presented in Fig. 1(d), where it operates at 2.7 GHz with a fractional bandwidth of 18.8% and a relatively large insertion loss. It is simulated on an RT/Duroid 5880 substrate with $\epsilon_r = 2.22$, $h = 0.7874$ mm.

$$L_d C_p C_d (L_a + L_b) \ll 1 \Rightarrow \omega_o \approx \sqrt{\frac{2L_d C_p + L_a + L_b}{4L_d C_p C_d (L_a + L_b)} \left(1 \pm \sqrt{1 - \frac{2L_d C_p^2 C_d (L_a + L_b)}{(2L_d C_p + L_a + L_b)^2}}\right)}$$

$$\sqrt{\frac{2L_d C_p^2 C_d (L_a + L_b)}{(2L_d C_p + L_a + L_b)^2}} \ll 1 \Rightarrow \omega_o \approx \sqrt{\frac{2L_d C_p + L_a + L_b}{2L_d C_p C_d (L_a + L_b)}} = \sqrt{\frac{1}{C_d (L_a + L_b)} + \frac{1}{2L_d C_p C_d}} \quad (3)$$

According to Eq. (3), the resonant frequency depends on patch capacitor (C_p), coupled line (C_d and L_d), and the stubs with the physical lengths l_1 , l_3 , l_4 and l_6 , which are modeled by L_a and L_b . To find more effective parameters, we apply a new approximation as follows:

$$L_a + L_b \gg 2L_d C_p \Rightarrow \omega_o \approx \sqrt{\frac{1}{2C_d L_d C_p}} \quad (4)$$

Equation (4) shows that coupled lines and patch cells are the most important parameters in determining the resonant frequency. Due to having the angular resonance frequency in GHz, the coupling capacitor should be large. Therefore, we have to choose the dimensions of patch cells somewhat large, while we are careful to save the overall size. Then, the space between coupled lines and the

In other to control the bandwidth of the proposed resonator, an optimization method can be performed. We can calculate the highest -3 dB cut-off frequency. Hence, obtaining the network function $H(j\omega_o)$ is essential. When the maximum amplitude $|H(j\omega_o)|$ is reduced to $0.707|H(j\omega_o)|$, we get the cut-off frequency. Finally, the dimensions must be tuned to obtain the highest cut-off frequency. Applying the optimization method shows that the bandwidth can be controlled by adjusting the patches. Figures 2(a)–(c) depict the bandwidth as a function of the dimensions of patch cells. The data obtained from Fig. 2 show that selecting the smaller patch cell can improve the bandwidth and insertion loss.

By adding two rectangular patches inside the proposed resonator, a BPF is designed as shown in Fig. 3(a). The corresponding dimensions of the proposed BPF (in mm)

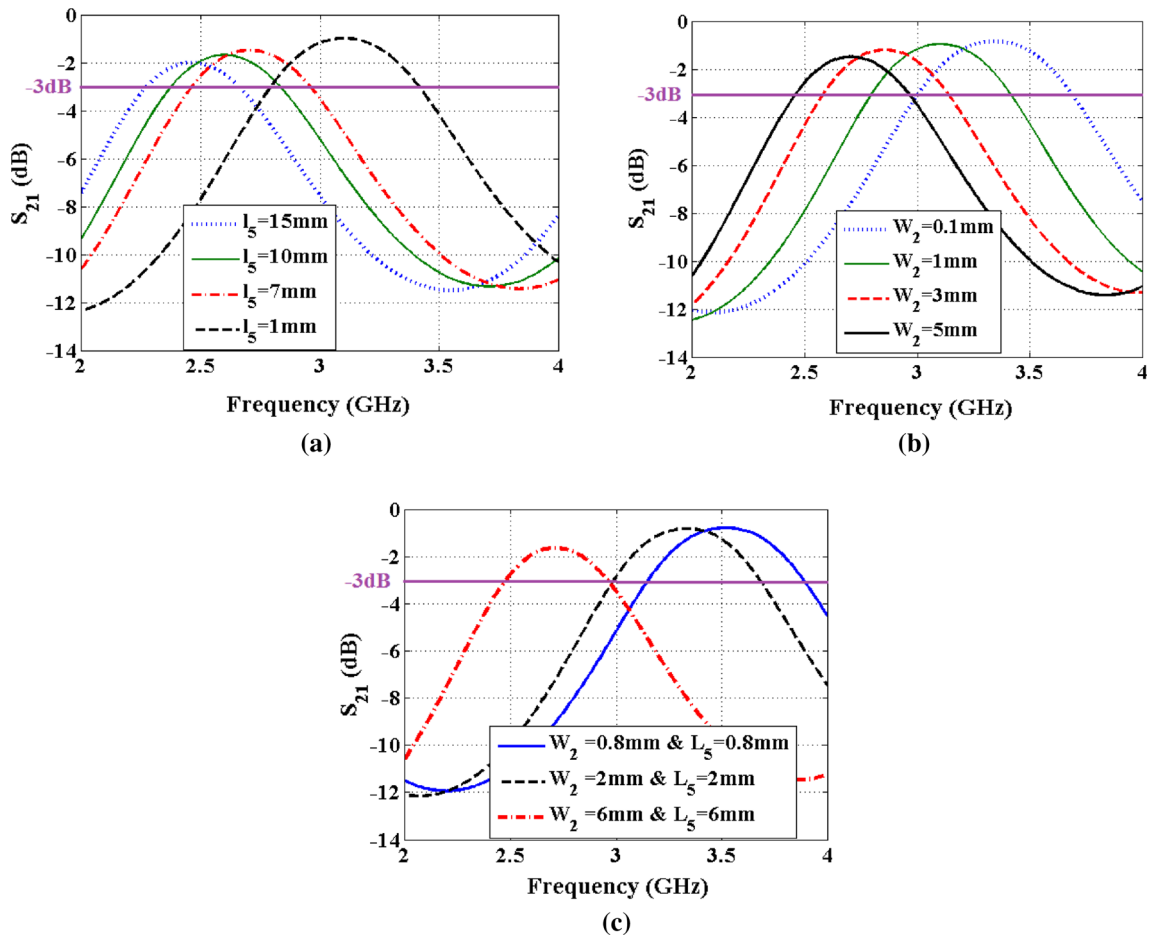


Fig. 2 Frequency response of the resonator as a function of: a l_5 , b w_2 , and c l_5 and w_2

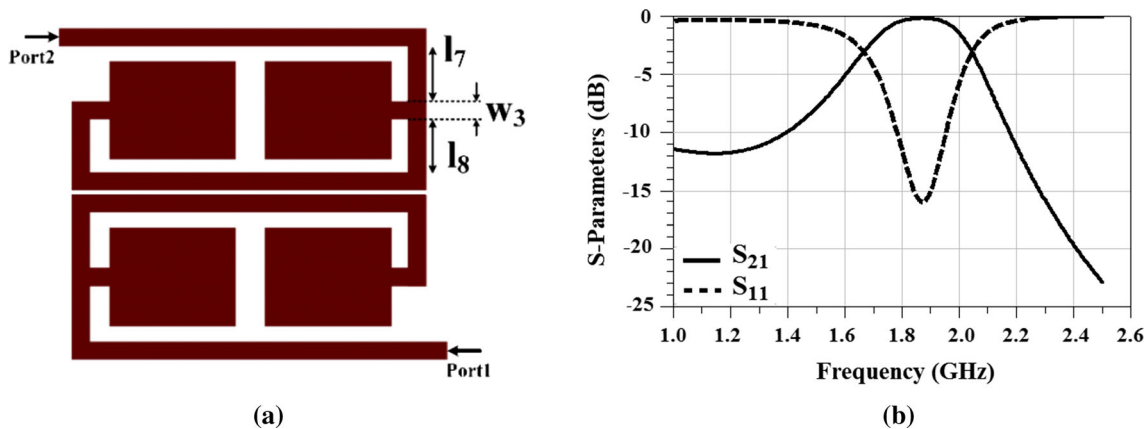


Fig. 3 Proposed BPF: a layout configuration, and b frequency response

are listed in Table 1. The other dimensions are exactly in accordance with the proposed resonator. Figure 3(b) depicts the frequency response of the proposed BPF. It operates at 1.87 GHz with a wide fractional bandwidth of 20.3% and a low insertion of 0.17 dB. It is clear that adding two rectangular patches can improve the frequency response without size increasing.

3 Diplexer design using ANN

In this section, we propose an accurate ANN model for designing a microstrip diplexer. As mentioned before, to tune the resonant frequency of the proposed BPF the best method is changing of the effective lengths and widths of microstrip cells used in the BPF layout. Therefore, if we

Table 1 Dimensions of the proposed BPF in mm

Parameter	l_1	l_2	l_3	l_4	l_5	l_6
Value	18.8	16.5	3	1.8	7	6.8
Parameter	l_7	l_8	w_1	w_2	w_3	s_1
Value	3	3	0.8	5	0.8	0.2

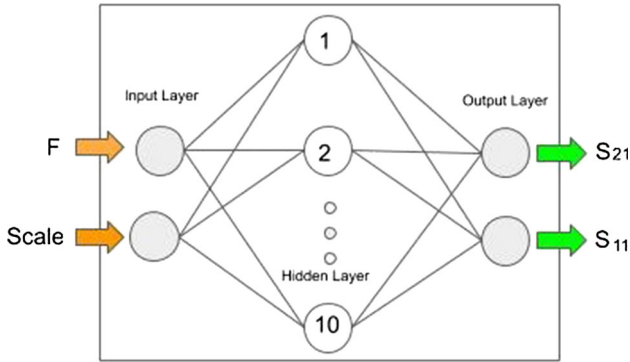


Fig. 4 Proposed MLP network

change the overall scale of the BPF dominations all effective lengths and widths of microstrip cells used in the BPF layout are changed subsequently. Thus, we selected frequency (per GHz) and the scale of the BPF dominations

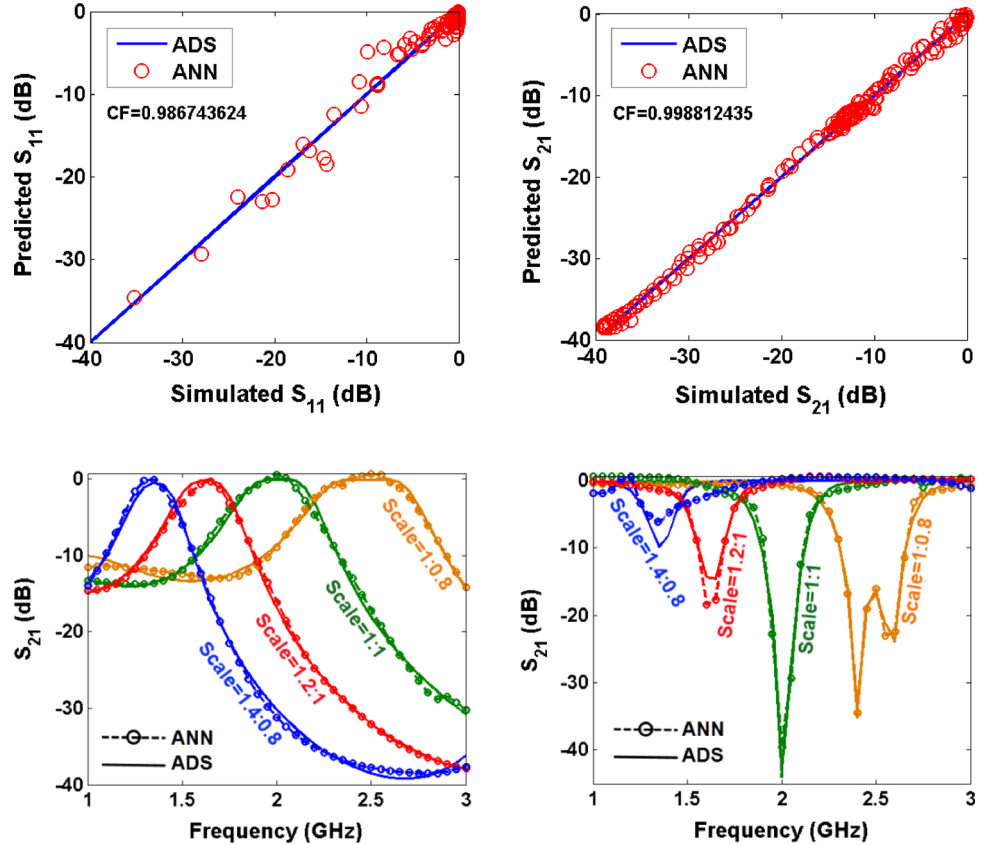
as the inputs and S-parameters (scattering parameters) i.e. S_{11} and S_{21} as the outputs of the proposed ANN model.

As shown in Fig. 4, a multilayer perceptron (MLP) neural network model is used which is the most used ANN. The presented MLP network has three layers i.e. input, hidden and output. More details about MLP neural networks can be found in [27, 28].

To develop the MLP model, a set of about 2000 data is used as the training and testing data. The data set is obtained by ADS full-wave EM simulator. About 70% of the data set is used for training and the rest is used to test and validate the proposed model. To build the best ANN model the main issue was to obtain an MLP network with high accuracy and less complicated structure. For this purpose, we tested many MLP structures with one and two hidden layers. Also, we changed the number of neurons in each hidden layers from 2 to 15 and the number of epochs from 50 to 500. Trainlm algorithm was chosen as the adaption learning function for all tested ANNs. At the end of this process, the best MLP network was obtained after 200 epochs with ten neurons in one hidden layer.

Figure 5 shows the obtained results of the proposed MLP model. In this figure, CF (correlation coefficient) is given by the following equation:

Fig. 5 Results of the proposed MLP model in comparison with ADS software



$$CF = 1 - \left[\frac{\sum_{i=1}^N (X_i(Sim) - X_i(Pred))^2}{\sum_{i=1}^N (X_i(Sim))^2} \right] \tag{5}$$

Where N is the number of data and ‘X(Simp)’ and ‘X(Pred)’ are the simulated (ADS) and predicted (ANN) values, respectively. As shown in Fig. 5, the MLP results are very close to the simulation results which show the proposed ANN model is very accurate.

Since ANN is a mathematical approach, we can obtain two equations for S₂₁ and S₁₁ based on the proposed MLP model:

$$\begin{aligned} S_{21} = & -0.74 * \text{Tansig}(-25.2 * F + 28.5 * \text{Scale} + 43.93) - 8.85 * \text{Tansig} \\ & \times (-0.29 * F - 1.87 * \text{Scale} + 3.285) - 0.83 * \text{Tansig} \\ & \times (-9.00 * F + 30.9 * \text{Scale} - 16.51) \\ & + 1.68 * \text{Tansig}(18.95 * F - 32.4 * \text{Scale} - 21.30) \\ & + 1.6493 * \text{Tansig}(-13.9 * F - 27.7 * \text{Scale} + 55.80) \\ & + 0.98 * \text{Tansig}(-37.1 * F + 91.3 * \text{Scale} + 12.95) \\ & + 2.95 * \text{Tansig}(14.63 * F + 28.1 * \text{Scale} - 57.24) \\ & + 43.6 * \text{Tansig}(-2.84 * F - 3.05 * \text{Scale} + 8.255) \\ & + 33.5 * \text{Tansig}(-1.27 * F - 3.44 * \text{Scale} + 6.462) \\ & + 57.3 * \text{Tansig}(3.020 * F + 4.25 * \text{Scale} - 9.643) - 20.6 \\ S_{11} = & -11.1 * \text{Tansig}(-25.2 * F + 28.5 * \text{Scale} + 43.93) \\ & + 6.10 * \text{Tansig}(-0.29 * F - 1.87 * \text{Scale} + 3.285) \\ & + 0.86 * \text{Tansig}(-9.00 * F + 30.9 * \text{Scale} - 16.51) \\ & - 24.2 * \text{Tansig}(18.95 * F - 32.4 * \text{Scale} - 21.30) \\ & - 109.07 * \text{Tansig}(-13.9 * F - 27.7 * \text{Scale} + 55.80) \\ & - 12.5 * \text{Tansig}(-37.1 * F + 91.3 * \text{Scale} + 12.95) \pm 109 * \text{Tansig} \\ & \times (14.63 * F + 28.1 * \text{Scale} - 57.24) - 8.14 * \text{Tansig} \\ & \times (-2.84 * F - 3.05 * \text{Scale} + 8.255) - 4.33 * \text{Tansig} \\ & \times (-1.27 * F - 3.44 * \text{Scale} + 6.462) - 9.42 * \text{Tansig} \\ & \times (3.020 * F + 4.25 * \text{Scale} - 9.643) - 2.90 \end{aligned} \tag{6}$$

Where Tansig is the transfer function for the hidden layer given by the following equation:

$$\text{Tansig}(x) = \frac{2}{1 + e^{-2x}} - 1 \tag{7}$$

The main advantage of the presented ANN model is its ability to calculate the outputs in a very short time. For example, if a simulation in ADS software takes few minutes to run; the proposed MLP network can do it in about 1 ms for the same condition. With this ability we can test many different microstrip layouts using the ANN method in a short time to obtain the best response for a special application. Using this method, we used the proposed MLP network to obtain two high-performance BPFs and place them into a single structure as a diplexer.

The proposed diplexer with its corresponding dimensions in mm is presented in Fig. 6. The designed diplexer

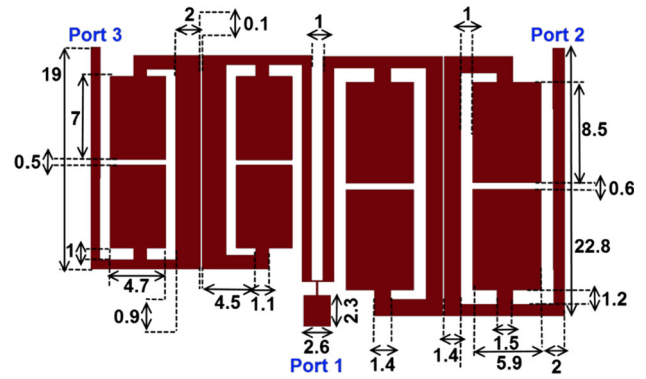


Fig. 6 Layout of the proposed diplexer

includes two similar filters that their basic structures have already been analyzed and explained. These filters are integrated with a simple T-junction structure.

4 Simulation and measurement results

We used ADS full-wave EM simulator and MATLAB software to design and simulate the proposed diplexer. The designed diplexer is implemented on an RT/Duroid 5880 substrate with $\epsilon_r = 2.22$, $h = 0.7874$ mm and $\tan(\delta) = 0.0009$. The measurements are done by Agilent network analyzer N5230A. The obtained S₂₁ and S₃₁ of the designed diplexer are shown in Fig. 7(a), whereas, Fig. 7(b) depicts the isolation and S₁₁ with a photograph of the fabricated diplexer. The overall size of the diplexer is 40.5 mm × 23.7 mm = 0.054 λ_g^2 , where λ_g is the guided wavelength calculated at 1.6 GHz.

The -3 dB bandwidth of the first channel is from 1.47 to 1.74 GHz, while another -3 dB passband is from 2 to 2.23 GHz. The first resonant frequency is tuned at 1.6 GHz, which is located at the middle of passband with the simulated insertion and common port return losses of 0.1 dB and 33 dB respectively. The second resonance frequency is at 2.1 GHz, which is approximately located in the middle of passband with the simulated insertion and return losses better than 0.16 dB and 22 dB, respectively. The measured insertion losses are about 0.5 dB greater than the simulated results due to copper and junction losses. Both channels are wide, with the fractional bandwidths 16.8% and 11% that make it appropriate for wideband applications.

The results show that the isolation between channels is better than -22 dB. The performance and size of the proposed diplexer are compared with the previous diplexers in Table 2. In this table, IL, FBW and F_O are insertion loss, fractional bandwidth and operation frequency, respectively, where the indexes 1 and 2 indicate the first and second passbands, respectively. As depicted in

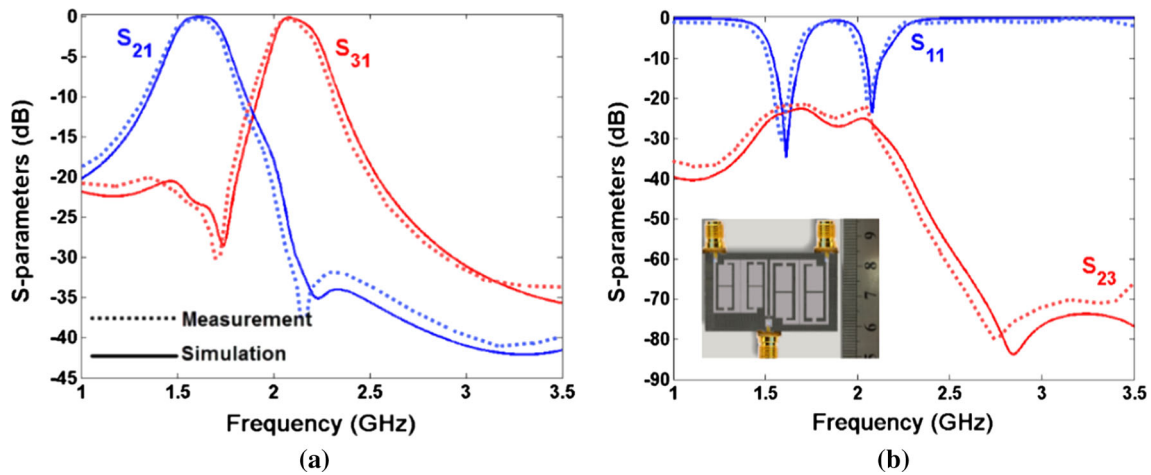


Fig. 7 Simulation and measurement results: **a** S_{21} and S_{31} , and **b** S_{11} , S_{23} and a photograph of the fabricated diplexer

Table 2 Comparison with the previous works (*: approximated values)

References	IL ₁ , IL ₂ (dB)	Size (λ_g^2)	FBW ₁ , FBW ₂	F _{o1} , F _{o2} (GHz)
This work	0.10, 0.16	0.054	16.8%, 11%	1.6, 2.1
[1]	0.2, 0.4	0.089	–	2.36, 4
[2]	0.18, 0.39	0.075	4%, 3.6%	2.4, 2.79
[3]	–	0.318	6%, 6.2%	1.84, 2.42
[4]	2.16, 2.24	0.116*	6.2%, 5.2%	1.8, 2.45
[5]	0.4, 0.42	0.095	–	1.8, 2.45
[6]	0.6, 0.9	0.081	–	2.6, 6
[7]	1, 0.9	0.127	6.1%, 5.8%	2.3, 2.72
[8]	1.43, 1.59	0.278	7.2%, 7.2%*	2.44, 3.52
[9]	1.5, 1.3	0.089	3.6%, 3.4%	2.3, 2.55
[10]	1.8, 1.5	0.705	8%, 9.2%	1.1, 1.3
[11]	2.8, 3.2	0.183	3.8%, 3.3%	1.5, 1.76
[12]	1.2, 1.5	0.137	3.59%, 3.2%	1.95, 2.14
[13]	2.2, 2.1	0.064	2%, 1.5%	1.8, 2.4
[14]	2.86, 3.04	0.689	3.6%, 3.6%	8, 9
[15]	2.35, 1.96	0.084*	6.1%, 7.4%	1.7, 2.49
[16]	1.4, 2.3	0.089	6.1%, 4%	1.05, 1.76
[20]	–	0.073	80%, 3.4%	3, 5.8

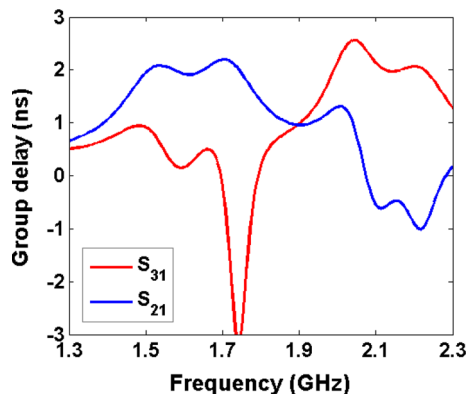


Fig. 8 Group delay of the proposed diplexer

Table 2, the minimum size, lowest insertion loss and widest fractional bandwidths are obtained in this work. Only the presented diplexer in [20] has a wider channel than our diplexer. However, another channel of this diplexer is narrow while it has a larger area and larger insertion losses.

Group delay is a type of distortion, which shows the phase linearity and passband flatness. However, there is no significant distortion as indicated by group delay < 10 ns while the insertion loss is low [29]. The group delay of the proposed diplexer is presented in Fig. 8. It shows that the maximum group delays at the first and second channels are 2.2 ns and 2.6 ns respectively. A comparison of the

Table 3 Group delay in comparison with previous works (MGD: maximum group delay; NCs: the number of channels)

Refs	This work	[6]	[20]	[29]	[30]	[31]	[32]
MGD	2.6 ns	3.15 ns	2 ns	3.67 ns	8 ns	2.5 ns	8 ns
NCs	2	2	2	3	4	2	3
Type	Diplexer	Diplexer	Diplexer	Filter	Filter	Filter	Filter

maximum group delays is shown in Table 3. As shown in this table, a good group delay is obtained in this work.

5 Conclusion

A compact microstrip diplexer with low insertion losses and wide FBWs was designed and fabricated using an accurate and fast artificial neural network model. The proposed diplexer consists of coupled lines loaded by patch cells; the patches could save size significantly. It has two flat channels with a maximum group delay of 2.6 ns. Therefore, the proposed diplexer can be used when we have high or low data rate communication links. Furthermore, the widest FBW obtained in the previous works was for one channel only, whereas, the obtained FBWs of the proposed diplexer in this work are 16.8% and 11% at the lower and upper channels, respectively. The passbands can cover L-Band and S-Band frequency spectrums. These advantages were obtained while the other parameters in terms of return losses, isolation and selectivity were acceptable.

Acknowledgements Authors would like to acknowledge the financial support of Kermanshah University of Technology for this research under grant number S/P/T/1177.

References

- Noori, L., & Rezaei, A. (2017). Design of a microstrip dual-frequency diplexer using microstrip cells analysis and coupled lines components. *International Journal of Microwave and Wireless Technologies*, 9(7), 1467–1471.
- Rezaei, A., Noori, L., & Mohamadi, H. (2017). Design of a novel compact microstrip diplexer with low insertion loss. *Microwave and Optical Technology Letters*, 59(7), 1672–1676.
- Feng, W., Gao, X., & Che, W. (2014). Microstrip diplexer for GSM and WLAN bands using common shorted stubs. *IET Electronics Letters*, 50(20), 1486–1488.
- Chinig, A., Zbitou, J., Errkik, A., Elabdellaoui, L., Tajmouati, A., Tribak, A., et al. (2015). A new microstrip diplexer using coupled stepped impedance resonators. *International Journal of Electronics and Communication Engineering*, 9(1), 41–44.
- Bui, D. H. N., Vuong, T. P., Allard, B., Verdier, J., & Benech, P. (2017). Compact low-loss microstrip diplexer for RF energy harvesting. *Electronics Letters*, 53(8), 552–554.
- Noori, L., & Rezaei, A. (2017). Design of a microstrip diplexer with a novel structure for WiMAX and wireless applications. *AEU-International Journal of Electronics and Communications*, 77, 18–22.
- Huang, F., Wang, J., Zhu, L., & Wu, W. (2016). Compact microstrip balun diplexer using stub-loaded dual-mode resonators. *IET Electronics Letters*, 52(24), 1994–1996.
- Xiao, J., Zhu, M., Li, Y., Tian, L., & Ma, J. G. (2015). High selective microstrip bandpass filter and diplexer with mixed electromagnetic coupling. *IEEE Microwave and Wireless Components Letters*, 25, 781–783.
- Salehi, M. R., Keyvan, S., Abiri, E., & Noori, L. (2016). Compact microstrip diplexer using new design of triangular open loop resonator for 4G wireless communication systems. *AEU International Journal of Electronics and Communications*, 70(7), 961–969.
- Chen, D., Zhu, L., Bu, H., & Cheng, C. (2015). A novel planar diplexer using slot line-loaded microstrip ring resonator. *IEEE Microwave and Wireless Components Letters*, 25(11), 706–708.
- Chen, C.-F., Huang, T.-Y., Chou, C.-P., & Wu, R.-B. (2006). Microstrip diplexers design with common resonator sections for compact size, but high isolation. *IEEE Transactions on Microwave Theory and Techniques*, 54(5), 1945–1952.
- Guan, X., Yang, F., Liu, H., & Zhu, L. (2014). Compact and high-isolation diplexer using dual-mode stub-loaded resonators. *IEEE Microwave and Wireless Components Letters*, 24(6), 385–387.
- Jun-Mei, Y., Zhou, H.-Y., & Cao, L.-Z. (2016). Compact diplexer using microstrip half—and quarter wavelength resonators. *Electronics Letters*, 52(19), 1613–1615.
- Cheng, F., Lin, X., Song, K., Jiang, Y., & Fan, Y. (2013). Compact diplexer with high isolation using the dual-mode substrate integrated waveguide resonator. *IEEE Microwave and Wireless Components Letters*, 23, 59–61.
- Chinig, A. (2017). A novel design of microstrip diplexer using meander-line resonators. *International Journal of Electronic Engineering and Computer Science*, 2(2), 5–10.
- Feng, W., Zhang, Y., & Che, W. (2017). Tunable dual-band filter and diplexer based on folded open loop ring resonators. *IEEE Transactions on Circuits and Systems*, 64(9), 1047–1051.
- Rezaei, A., Noori, L., & Jamaluddin, M. H. (2019). Novel microstrip lowpass-bandpass diplexer with low loss and compact size for wireless applications. *AEU International Journal of Electronics and Communications*, 101, 152–159.
- Rezaei, A., Noori, L., & Mohammadi, H. (2019). Design of a miniaturized microstrip diplexer using coupled lines and spiral structures for wireless and WiMAX applications. *Analog Integrated Circuits and Signal Processing*, 98(2), 409–415.
- Rezaei, A., Noori, L., & Jamaluddin, M. H. (2019). Design of a novel microstrip four-channel diplexer for multi-channel telecommunication systems. *Telecommunication Systems*, 1, 1–9. <https://doi.org/10.1007/s11235-019-00563-x>.
- Deng, H. W., Zhao, Y. J., Fu, Y., Ding, J., & Zhou, X. J. (2013). Compact and high isolation microstrip diplexer for broadband and WLAN applications. *Progress In Electromagnetics Research*, 133, 555–570.
- Chae, Y. T., Horesh, R., Hwang, Y., & Lee, Y. M. (2016). Artificial neural network model for forecasting sub-hourly electricity usage in commercial buildings. *Energy and Building*, 111, 184–194.

22. Moayedi, H., & Rezaei, A. (2019). An artificial neural network approach for under-reamed piles subjected to uplift forces in dry sand. *Neural Computing and Applications*, 31(2), 327–336.
23. Salehi, M. R., Noori, L., & Abiri, E. (2016). Prediction of matching condition for a microstrip subsystem using artificial neural network and adaptive neuro-fuzzy inference system. *International Journal of Electronics*, 103(11), 1882–1893.
24. García, J. P., Pereira, F. Q., Rebenaque, D. C., Díaz, J. S. G., & Melcón, A. Á. (2009). A new neural network technique for the design of multilayered microwave shielded bandpass filters. *International Journal of RF and Microwave Computer-Aided Engineering*, 19(3), 405–415.
25. Tomar, G., Kushwah, V. S., & Bhadauria, S. S. (2013). Artificial neural network design of stub microstrip band-pass filters. *International Journal of Ultra Wideband Communications and Systems*, 1, 38–49.
26. Noori, L., & Rezaei, A. (2017). Design of microstrip wide stopband quad-band bandpass filters for multi-service communication systems. *AEU-International Journal of Electronics and Communications*, 81, 136–142.
27. Hagan, M. T., Demuth, H. B., & Beale, M. H. (2004). *Neural network design*. Beijing: China Machine Press.
28. Hornik, K., Stinchcombe, M., & White, H. (1989). Multilayer feedforward networks as universal approximators. *Neural Networks*, 2(5), 359–366.
29. Wibisono, G., Firmansyah, T., & Syafraditya, T. (2016). Design of triple-band bandpass filter using cascade tri-section stepped impedance resonators. *Journal of ICT Research and Applications*, 10(1), 43–56.
30. Lin, S.-C. (2011). Microstrip dual/quad-band filters with coupled lines and quasi-lumped impedance inverters based on parallel-path transmission. *IEEE Transactions on Microwave Theory and Techniques*, 59(8), 1937–1946.
31. Sarkar, P., Ghatak, R., & Poddar, D.-R. (2011). A dual-band bandpass filter using SIR suitable for WiMAX band. In *International conference on information and electronics engineering IPCSIT* (vol. 6, pp. 70–74).
32. Liu, Y. (2010). A tri-band bandpass filter realized using tri-mode T-shape branches. *Progress in Electromagnetics Research*, 105, 425–444.

Publisher's Note Springer Nature remains neutral with regard to jurisdictional claims in published maps and institutional affiliations.



A. Rezaei Assistance Professor of Electrical Engineering in Kermanshah University of Technology. Abbas Rezaei received the B.Sc., M.Sc. and Ph.D. in electronics engineering from Razi University, Kermanshah, Iran, in 2005, 2009 and 2013, respectively. His current research interests include RF and microwave circuits, computational intelligence and nanotechnology.



he presented many conference papers. His current research interests include antenna design, numerical RF dosimetry, MW measurement and MW components design. Prof. Yahya is a regular reviewer of the Electromagnetics Academy, Cambridge, USA, PIERS Journals publications, since 2009, Science and Engineering of Composite Materials journal and International Journal of Applied Electromagnetics and Mechanics.



L. Noori received her B.Sc. and M.Sc. degrees in electronic engineering from Razi University, Kermanshah, Iran in 2005 and 2009 respectively. She received her Ph.D. in electronic engineering at the Shiraz University of Technology. Her research interests focus on artificial microstrip coupler, microstrip filter, neural networks and LNAs.



Mohd Haizal Jamaluddin received bachelor's and master's degrees in Electrical Engineering from Universiti Teknologi Malaysia (UTM), Malaysia, in 2003 and 2006, respectively, and the Ph.D. degree in signal processing and telecommunications from the Université de Rennes 1, France, in 2009, with a focus on microwave communication systems and specially antennas such as dielectric resonator and reflect array and dielectric dome antennas. He is currently an Associate Professor with the Wireless Communication Centre, School of Electrical Engineering, Universiti Teknologi Malaysia. His research interests include dielectric resonator antennas, printed microstrip antennas, MIMO antennas and DRA reflectarray antennas. He has published more than 100 papers in reputed indexed journals and conference proceedings.